Thermodynamic Approach to Describe the Martensite Phase Transformation Kinetics via the Stabilization of Austenite

Steve Gaudez, Juan Macchi, Guillaume Geandier, Sabine Denis, Sebastien Y.P. Allain

Thermodynamic approach to describe the martensite phase transformation kinetics via the stabilization of austenite

Steve Gaudez[1,*], Juan Macchi[1,**], Guillaume Geandier[1], Sabine Denis[1], Sébastien Y.P. Allain[1]

[1] Institut Jean Lamour, UMR 7198 CNRS-Université de Lorraine, 54011 Nancy, France

Corresponding author emails: * steve.gaudez@psi.ch, ** juan.macchi@univ-rouen.fr

Keywords
Steel; Martensite transformation; Thermodynamics; Kinetic; Austenite grain size; Stress effect; Composition

Abstract
This study investigated the spread of the martensite transformation, i.e., the extent of the transformation as a function of the temperature, via the development of a model focusing on the stabilization of residual austenite along the transformation rather than describing the nucleation processes of each individual unit of martensite. The stabilization of the retained austenite is described in a thermodynamic framework accounting for the chemical composition, grain sizes, stress state, dislocation density, and temperature effects. *In situ* X-ray diffraction experiment was performed at synchrotron PETRA III (Hamburg, Germany) on a low-alloyed steel to support the theoretical development. Among others, the martensite transformation kinetic as well as the lattice parameter and dislocation density of austenite were measured during the transformation. In order to describe the refinement of austenite grains during the transformation the initial prior austenite grain size distribution was determined by thermal etching. A good agreement of up to 60-70% of the martensite transformation upon cooling is found between the results of the model and the experiment. The results show that the major contribution to the spread of the transformation is the austenite refinement during the transformation itself. For higher martensite fractions the discrepancy observed is attributed to the simple description of austenite refinement used. In addition, the spread of the martensite transformation is shown to be linked with the change of the chemical driving force related to the steel composition, with the C showing the highest effect. New coefficients, based on numerical calculations, for the rate parameter (α) of the martensite transformation were proposed.

1 Introduction

Martensite is a hard phase found in quenched iron alloys [1,2] and also in other metals such as Zr [3], Co [4], and Ti [5] alloys. Martensite has been used since the beginning of the Iron Age to harden swords [6, 7] and is still presently used in many applications essential to daily life (e.g., energy [8], surgical [9], and automobile [10]). Despite a long history, this phase is still the subject of intense research as it is a key constituent of most of the advanced high-strength steels for automotive construction, such as dual phase or quenching and partitioning steels; it is also the main constituent of press-hardened steels after forming (boron steels) [11, 12] and tempered martensite is often found in the field of energy production and transport (nuclear vessel, pipelines, etc.). In iron alloys, martensite is a metastable product of austenite decomposition by a displacive transformation. In low-alloyed steels, it is obtained after a fast cooling from the austenitic domain at high temperature down to room temperature or below. In steels, mainly two types of martensite are reported; namely ε and α' martensites. In the following, only the α' martensite will be considered, as ε martensite is not observed in low-alloyed steels (even as an intermediate decomposition product like in some highly alloyed steels). Although for extremely fast transformation the formation of twinned martensite has been observed even in low-carbon steels, the mentioned cooling rates are not the scope of the present study [13]. In addition, the martensite transformation considered here concerns carbon steels with carbon content lower than $\sim$0.6 wt% and with a lath morphology [13]. The transformation mechanism including the hexagonal close-packed (HCP) as an intermediate phase during the face-centered cubic (FCC) to body-centered cubic (BCC) martensite transformation is not accounted for in the present model as it is restricted to low-alloyed steels and the transition is usually observed for

high-alloyed steels. However, it can be mentioned that mono-layers of HCP have been predicted in pure Fe as an intermediate phase during the martensite transformation for particular interface conditions via molecular dynamics simulation under [14–16] which could affect the kinetics of the transformation.

Martensite (α') transformation occurs by cooperative atomic movements without long-range diffusion from the FCC to BCC phase and leads locally (at the scale of the lath) to a volume expansion (∼2-4 % depending on temperature and carbon content) and to a shear (∼20-25 %). Let us mention that recent works [17, 18] are re-discussing the well-known shear mechanism of the classical theories of the crystallography of martensitic transformation [19] by introducing an angular distortion and lattice distortion wave to explain the transformation and the observed orientation relationship. In carbon steels, the product phase is not cubic due to the reordering of carbon atoms in preferential directions at short range in the lattice (called Zener ordering), leading to a distortion of the cubic lattice [20]. It is also well known that the transformation strains (shear and volume variation) lead to internal stresses both in austenite and martensite that are accommodated by different mechanisms (elastic strains, plastic strain in the parent phase, self-accommodating laths, and internal defects in the martensite such as dislocations and twins) [21–25] to relax the stresses.

The martensitic transformation is possible, from the thermodynamic point of view, because the driving force to initiate the $\gamma \rightarrow \alpha$' transformation is sufficiently high at low temperature without the possibility to initiate any diffusional transformation; prior ferrite/pearlite/bainite nucleation and growth must have been avoided by sufficiently rapid cooling. The degree of undercooling necessary to initiate the transformation is controlled by an energy barrier which accounts for the creation of an interface between the martensite and the parent phase and its associated energy, the deformation energies as well as a thermal frictional work related to the alloying elements [26–28]. The martensitic transformation thus starts at a critical temperature when the driving force for transformation is higher than the barrier. This critical temperature is known as the martensite start temperature (Ms). For most of the steels, the martensite transformation is considered time-independent and the progress of the transformation depends solely on the temperature reached below Ms. The higher the degree of undercooling, the higher the transformation fraction. In most steels the transformation takes place over a wide temperature range; it can be mentioned as counterexamples that high nickel alloyed steels present a sudden burst of the martensite phase fraction at Ms, e.g., [29, 30]. A large difference between the Ms and Mf (martensite finish) temperatures is observed (∼200 °C in low-alloyed steels). This phenomenon is known as the spread of martensite transformation.

The spread of martensite transformation is explained by the self-stabilization of the untransformed austenite during the progress of the transformation and thus during cooling [31]. Retained austenite is stabilized from the thermodynamical point of view mainly by micromechanical effects. During martensitic transformation, austenite develops a mean hydrostatic pressure [23,32]. Nakada *et al.* [23] investigated for instance the hydrostatic pressure in retained austenite by X-ray diffraction in a Fe-Ni alloy and reported that the hydrostatic pressure resulting from the transformation is not large enough to explain the austenite stability and the spreading of the martensite transformation according to the description of Patel and Cohen [33]. This group of authors suggests that other mechanisms are required, that could be related to the size of retained austenite (size effects) [20], which is accounted for the prediction of the martensite start temperature, e.g., [34]. The evolution of the chemical composition, mainly carbon content, of austenite is also possible during the transformation by a partitioning mechanism from the martensite to the surrounded austenite as proposed in [35]. However, according to carbon partitioning simulations at 350 °C [36] and the cooling rate used during the martensite transformation in [35], (∼40 °C/s Figure 5 in [35]), carbon partitioning from martensite to retained austenite during fast quenching is of second order in most conditions and will not be taken into account in the present approach. Nevertheless, carbon redistribution within the martensite phase (segregations, clusters, and carbides) occurs during the transformation [37] and could affect the austenite stability. In addition, even if the transformation is possible, the martensite/austenite interface mobility can be drastically reduced due to the presence of defects as dislocations [31, 38], twins, pre-existing martensite platelets, or precipitates (reduction of the mean free path in the microstructure).

It should be pointed out that Koistinen and Marburger already mentioned that the complete martensite transformation cannot be achieved by cooling [39] (i.e., the Mf temperature does not strictly exist), which means that retained austenite is thus strongly stabilized during the transformation. In their seminal work, they proposed a phenomenological description of the volume fraction of martensite as a function

of the undercooling below Ms, the well-known Koistinen-Marburger equation [39]:

$$y = 1 - \exp(-\alpha(Ms - T)) \tag{1}$$

where y is the transformed volume fraction, α is the rate parameter, Ms is the martensite start temperature, and T is the temperature. This equation was improved in order to take into account the alloying elements and the mean prior austenite grain size on the kinetics rate parameter (α) [31, 40, 41].

The modeling approach proposed in the present work is original as it focuses on the stabilization of residual austenite along the transformation through a thermodynamic approach taking into account the chemical composition, grain sizes, stress state, dislocation density, and temperature effects. According to [31], these effects were not all considered together to describe the martensite transformation before. In comparison with the approaches describing nucleation processes of each individual unit of martensite [42, 43], the auto-catalytic nature of martensite nucleation is accounted for. Indeed, the martensitic transformation is assumed to progress by the successive appearance of martensite packets in retained austenite domains, thus containing already self-accommodating variants. It aims to describe the fundamental scattered nature of martensite, which has recently been highlighted in the description of the work-hardening of this phase [44–47]. This is why a class model based on the size distribution of austenite grains has been used as a starting point. The proposed theoretical development relies on the experimental results gathered on low-alloyed steel as some contributions are not convincingly modeled in the literature so far (e.g., austenite stress state). However, the model developed is more general and can be applied, as will be shown in the final discussion, on a larger panel of martensitic steels.

In the present study, the martensite transformation kinetic is investigated experimentally with *in situ* high energy X-ray diffraction in low-alloyed carbon steel. A numerical model based on thermodynamic and experimental results was developed to investigate and understand the martensite transformation kinetics and its governing mechanisms at the microstructure scale. This permitted us to identify and quantify the contributions of the different stabilizing factors of austenite during the transformation and their impact on the progress of the transformation itself.

2 Material and methods

A low-carbon alloyed steel cold-rolled (thickness of 1.5 mm) with a composition reported as Fe-0.21C-0.25Si-1.8Mn-0.2Cr wt% (Fe-0.989C-0.49Si-1.83Mn-0.19Cr at%) provided by ArcelorMittal Maizières Research (France) was investigated. Martensite transformation was followed *in situ* by high energy X-ray diffraction (HEXRD) at the Deutsche Elektronen Synchrotron (DESY, PETRA-III) P07 beam line in transmission mode (E = 100 keV, λ = 0.12398 Å, beam size = 400×400 µm^2). The diffracted Debye-Scherrer rings were recorded thanks to a fast 2D Perkin Elmer XRD 1621 Flat Panel detector with an acquisition rate of 10 Hz and an exposure time of 0.1 s, a frequency needed to study the martensite transformation with a sufficient time resolution. The thermal treatment (austenitization and quench) was performed with a modified Bärh DIL805 A/D dilatometer available at the beamline. The sample was austenitized at 880 °C during 180 s and then argon gas quenched with a cooling rate of 40 °C/s for temperatures above $T > 300$ °C and an average cooling rate of 20 °C/s below down to room temperature. The recorded Debye-Scherrer rings during the thermal treatment were integrated circularly with the pyFAI python library [48] to obtain radial line profiles (intensity vs. 2θ). These line profiles were then analyzed using the Rietveld method with the FullProf software. Two phases were considered during the Rietveld analysis of the diffraction patterns: martensite (α') with a body-centered tetragonal structure (I4/mmm) and austenite (γ) with a cubic face-centered structure (Fm-3m). The dislocation density in austenite was investigated during the martensite transformation following the modified Williamson-Hall method [24]. The instrumental broadening was evaluated with a silicon powder reference and subtracted from the measured width of the observed peaks. More information on the *in situ* HEXRD experiment and its analysis can be found in [24].

The prior austenite grain boundaries were revealed by thermal etching [49] using the same austenitic heat treatment on another sample. Before thermal etching, the sample was ground down to mirror finishing to remove the oxide and decarburized layers that could be present at the surface after industrial processes. Austenite grain boundaries were then investigated by optical microscopy to quantify the distribution of the prior austenite grain size (PAGS) by measuring the area of each observed grain. Then,

the measured areas were converted into equivalent diameters assuming a disk shape. More than 500 grains were considered in total.

3 Results

Figure 1 shows (a) an optical micrograph of the studied steel after thermal etching and (b) the measured prior austenite grain size distribution obtained after quenching from the austenitic domain. On the micrograph, grain boundaries are visible as dark contrasted lines delimitating prior austenite grains. In total, more than 500 grains were manually identified and outlined from different regions of one sample. The measured surface of each grain was then used to calculate the area equivalent diameter. The PAGS present a homogeneous size, i.e., without obvious coarse grains resulting from an exaggerated growth. Their sizes were investigated and they present a regular distribution with a skewness toward the larger areas. This distribution was fitted with a log-normal distribution, leading to a mean PAGS of 4.8 µm with a standard deviation of 2.3 µm.

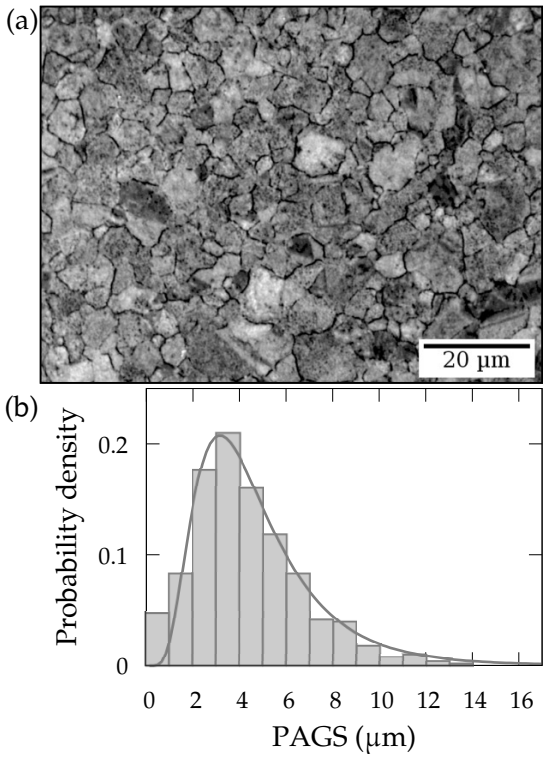

Figure 1: (a) Optical micrograph of the steel after thermal etching and (b) PAGS distribution and the fitted log-normal probability density function obtained after the martensite transformation.

Figure 2 shows (a) the martensite transformation kinetics and the measured austenite lattice parameter as a function of the temperature and (b) the mean austenite dislocation density as a function of the martensite phase fraction, both obtained via *in situ* HEXRD. As reported in [24] the martensite transformation presents two steps that are common in industrial steels: first, a sluggish transformation starting at 400 °C followed by a rapid one below 365 °C. The phase fraction reported at the transition is low (5 wt%). The experimental value that will be considered in the following is Ms = 365 °C [24] since it is representative of the alloy mean composition and mean PAGS according to [34]. The slight increase before the main transformation is attributed to a possible negligible bainite/martensite transformation in micro-segregated domains with a lower hardenability or to a decarburized layer at the surface. The fraction of martensite obtained at room temperature is 96±1 wt% and the remaining fraction is retained austenite with a mean dislocation density close to $10^{15}/m^2$ (Figure 2b). After martensite transformation, at room temperature, there is no detectable presence of cementite or transition carbides from the diffraction line profiles. During the cooling from the austenitizing temperature (880 °C) down to the martensite start temperature (365 °C), the average austenite lattice parameter follows a linear trend. The same

trend is kept up to ∼60 wt% of formed martensite. The stress-free austenite lattice parameter (a_0^γ) was fitted in the temperature range 400 to 880 °C with a temperature dependence function suggested by [50]:

$$CTE = B^\gamma \left[1 - \exp\left(\frac{T}{\Theta^\gamma}\right)\right] \quad (2)$$

The reported coefficients are $B^\gamma = 2.4{\times}10^{-5}$/K and $\Theta^\gamma = 473$ K which are respectively the CTE (coefficient of thermal expansion) at high temperature and the Debye temperature, the critical temperature above which the CTE can be considered as constant (i.e., $T \gg \Theta^\gamma$). The parameters were obtained by the adjustment of the austenite lattice parameter. The B^γ is close to the values reported in [50,51] while the Debye temperature agrees with the one reported in [52]. Below 320 °C, the austenite lattice parameter deviates from the linearity; the lattice parameter is lower than the fitted stress-free lattice parameter. It is observed that austenite goes in compression with the progress of the martensite transformation. Such an evolution has been already observed in different steels [23, 25, 32, 53, 54][1] and has been related to the development of compression hydrostatic stress state in austenite (the shear components cannot be revealed to the sole mean lattice parameter). Other studies showed an inversion of the austenite stress state with the progress of the martensite transformation, from tension to compression at a martensite fraction range between 20 and 30 % [51, 53, 55]. Although the mean tensile stresses observed can be easily understood considering the volume change from the austenite to martensite transformation and martensite being considered as an inclusion in austenite, the interpretation of the inversion and compression stresses is not straightforward. The mechanisms are not clearly understood in the literature but seem linked to mechanical interactions when forming martensite [54], the inversion of the percolation of austenite network [23, 55], and the contribution of crystal defects to the lattice parameter of the phase [32].

Considering the exponential dependence of the elastic strain-free austenite lattice parameter proposed by [50], the austenite remains in compression down to room temperature during the present experiment and the pressure increases up to P ≈ 1.2 GPa at room temperature ($P = 3\varepsilon_l^\gamma K$ where $\varepsilon_l^\gamma = (a_{exp}^\gamma - a_0^\gamma)/a_0^\gamma$ where a_{exp}^γ and a_0^γ are respectively the experimental and strain-free austenite lattice parameters and K the bulk modulus of austenite at RT). This determination of internal stresses in austenite depends on the choice of the CTE model. However, the hydrostatic pressure is not the main effect allowing to explain the martensite transformation kinetics and spread. This is due to the fact that the high value of hydrostatic pressure reported affects mainly the retained fraction of austenite present at the end of the transformation. During the transformation, the dislocation density in austenite increases (Figure 2b) due to the accommodation of the transformation strain (expansion and shear). The initial dislocation density in austenite (i.e., before the martensite transformation) is low and estimated at $\sim 0.16{\times}10^{14}$ /m^2 and increases up to $\sim 14{\times}10^{14}$ /m^2 at the end of the transformation, i.e, almost a hundred times the initial value. A similar order of magnitude of dislocation density in austenite has been reported recently in [32] confirming the high dislocation density reported here. Additional information on the mean dislocation density in austenite and martensite for the present transformation and alloy can be found in [24].

In the following, an approach has been developed and used to describe the progressive martensitic transformation as a function of the temperature to discuss the relative contributions of different factors contributing to the spread of the martensite transformation.

4 Modeling

During the cooling from the austenitic field, the diffusionless transformation from austenite to martensite phase becomes possible when the temperature is reduced below T_0 which characterizes the equality between the Gibbs free energies of the parent austenite phase and the product ferrite phase ($G^\gamma = G^\alpha$) considering the same composition in both phases. In the following, it will be explicitly assumed that martensite is described from the thermodynamical point of view as ferrite. The nucleation of a martensite plate is accompanied by a shape and volume change leading to internal stresses, i.e., deformation energies, and by the creation of an interface between the martensite and the austenite which oppose the transformation. These energies opposing the transformation, nucleation barrier or called here critical resistive force ($\Delta G_C^{\gamma\to\alpha}$), must be overcome by the chemical driving force (free energy change) related to a certain volume of martensite at temperature T ($\Delta G_{chem}^{\gamma\to\alpha}(T) = G^\gamma - G^\alpha$) which increases with the

[1] In [23] there is no experimental measurement up to ∼70 % of martensite phase fraction.

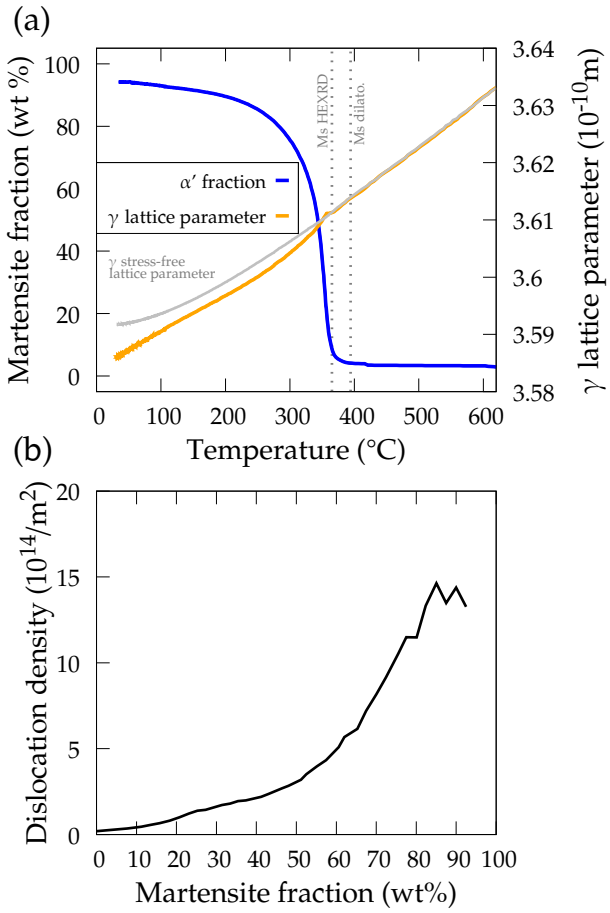

Figure 2: (a) Martensite transformation and austenite lattice parameters as a function of the temperature during the quenching, obtained via HEXRD experiment. The stress-free austenite lattice parameter fitted with Equation 2 is displayed. (b) Mean dislocation density in austenite as a function of the martensite fraction.

degree of undercooling $(T - T_0)$. The equality between the chemical free energy change and the critical resistive forces allows to obtain the martensite start temperature thanks to the following equation:

$$\Delta G^{\gamma\to\alpha}_{chem}(Ms) = \Delta G^{\gamma\to\alpha}_{C} \tag{3}$$

This thermodynamic description has been applied to estimate the temperature at which martensite transformation starts (Ms).

As a first simplified approach, the elastic strain energy associated with the formation of the first martensite plate (taken as an oblate spheroid with a given aspect ratio) can be calculated using Eshelby's theory (with a free strain composed of the volume variation and the shear) [56,57] and Ms can be evaluated with above criterion (interfacial energy can be neglected in comparison with deformation energies). The energy calculated is highly dependent on the martensite aspect ratio. The higher the ratio, the higher the energy is. Considering an aspect ratio of ∼0.2, the elastic energy is clearly over-estimated compared to the critical driving force needed to nucleate martensite, as shown by [56]. Only based on the elastic theory, an aspect ratio well below 0.05 is expected to initiate martensite transformation, while recent works report an aspect range ratio from 0.13 to 0.5 in steels [34, 58, 59]. The transformation is then possible only if the transformation strains are accommodated, in other words, if the self-accommodating blocks of laths nucleate at the same time to form packets. On the other hand, following a far more empirical way, several authors have proposed to calculate the Ms temperature as a function of the alloy composition and mean PAGS [26, 27, 31, 34].

"Real" austenite microstructures are far from being homogenous and present PAGS distribution or composition heterogeneities which lead to a distribution of local Ms temperatures. During the transfor-

mation, these initial distribution evolves (e.g., austenite size distribution due to the progressive austenite domain size reduction) and additional contributions (e.g., internal stresses) make vary the initial martensite start temperature distribution. As a consequence, after a certain amount of transformation, the Ms temperature of the remaining austenite has decreased compared to the initial austenitic microstructure even for a fixed mean alloy composition. The present theoretical development is based on this concept and will be sustained by our experimental results in the following.

4.1 Description of the model

4.1.1 Principle and implementation

In the present approach, the martensite transformation kinetics is calculated following an iterative approach. The principle is the following: when a first martensite fraction appears, it affects the remaining austenite whose $\Delta G_C^{\gamma\to\alpha}$ increases and whose Ms temperature decreases in turn. The transformation could only proceed with an additional driving force increment, i.e., if the $\Delta G_{chem}^{\gamma\to\alpha}(T)$ increases, which is made possible by a temperature decrease in order to reach the new Ms temperature. This transformation criterion is similar to the one used in previous works dealing with micromechanical approaches of martensitic transformation under stress in order to describe the progress of the transformation [60].

This scheme requires being able to estimate how the $\Delta G_C^{\gamma\to\alpha}$ evolves in each available austenite domain and to estimate the fraction of martensite transformed at each step. Before any transformation in austenite, the dislocation density is low and is supposed to be homogeneously distributed in PAGS and no significant internal stresses are expected at that stage. Experimentally, it has been shown that martensite does not start in all PAGS at the same time [61,62]. The transformation is localized in some grains, as the initial microstructure is already heterogeneous in terms of the size distribution (Figure 1). The largest austenite grains are the first to transform as the critical resistive force in these grains is lower, i.e., they present higher Ms temperatures than the smaller grains, due to the Hall-Petch strengthening effect. The martensite transformation occurring in these largest grains splits the PAGS by the formation of a first packet of blocks. The total transformed fraction is known and corresponds to the fraction of the grain transformed scaled by the probability of density of the corresponding mean grain size in the austenite grain size (AGS) distribution. The remaining austenite of the transformed grains forms new austenite domains with a far lower size. As a consequence, it leads to a change in the AGS distribution. During this martensite transformation increment, internal stresses will be also generated in the austenite as observed by the HEXRD experiments. The purpose of the model is to estimate how this size distribution and the mean stress of the remaining austenite evolve in order to calculate the new Ms temperature distribution.

In order to continue the transformation and to transform the new largest grains, a decrease in temperature is necessary to increase the chemical free energies change ($\Delta G_{chem}^{\gamma\to\alpha}|_T$) of all the austenite grains. A new increment of transformation is expected when this driving force exceeds the new recalculated critical resistive forces ($\Delta G_C^{\gamma\to\alpha}|_T$) in those largest austenitic grains. The kinetics is, then, only a function of the temperature, as expected for the studied transformations. These steps can be repeated until the quasi-full austenite transformation into martensite occurs.

Figure 3 details our procedure to track the evolution of the AGS and redistribute the untransformed austenite grains. The initial microstructure is only formed by austenite grains (empty and hatched domains). The transformation starts with the largest grain (step 0), which is split into two domains: martensite in red and remaining austenite (hatched '//' area) (step 1). The remaining austenite is, then, redistributed in the AGS distribution (step 1). Step n shows the microstructure and the AGS distribution after n repeated operations. The transformed fraction appears in red (darker red for the latter formed martensite) and the remaining smaller austenite domains are dispersed in the microstructure (some of these domains were initially present in the initial fully austenitic microstructures but most of them have been created by the progressive martensitic transformation). The grain-splitting process and the associated redistribution of the AGS as well as the evolution of the critical resistive forces will be detailed in the following sections.

4.1.2 Evolution of austenitic domains

To model the austenite grain splitting process, the fraction transformed at each step must be defined. For the largest grains, four martensite packets (blocks of parallel blocks of laths with the same habit plane) are generally observed. This number decreases toward one for the smallest grains [22,31,63,64] but remains

higher than one [64]. The change from multiple to nearly one single packet allows for maintaining the optimum aspect ratio of the martensite laths [34]. For carbon steels, the threshold value (denoted d_C^γ) for this change occurs in the range of 20 to 30 µm, 14 µm, and 11 µm according respectively to [34, 58, 64]. In the present study, to take into account the variation of the number of packets as a function of the austenite grain size the fraction transformed at each step is fixed at 50 % of the volume occupied by the considered austenitic domain for $AGS > d_C^\gamma$ while the fraction transformed at each step is fixed at 75 % of the volume occupied by the considered austenitic domain for $AGS \leq d_C^\gamma$. The particular two values (i.e., 50 % and 75 %) have been chosen according to the experimental results from low-alloyed steels presented in [64].

For simplification a two-dimensional approach was used: austenite grains are assumed circular and after a transformation, the remaining area is converted into an equivalent disc and is redistributed into the corresponding diameter of the AGS distribution as illustrated in Figure 4 (further details can be found in the Supplementary Material A). The evolution of the mean hydrostatic stress and dislocation density are evaluated from the experiment (Figure 2) and are a function of the sole fraction of martensite.

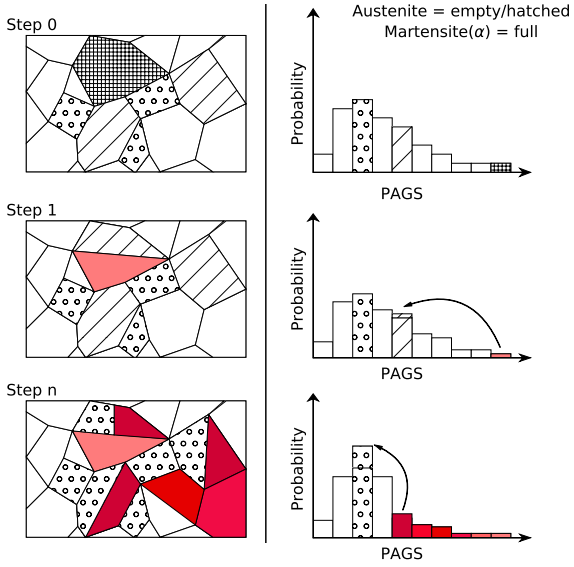

Figure 3: Schematic representation of the austenite grain splitting process by the martensite transformation (represented in red) and corresponding AGS at different steps.

4.1.3 Evolution of the critical force

In this section, the critical force for a given austenitic domain and its evolution during the transformation will be estimated. Several microstructural and mechanical contributions are considered and summed up:

$$\begin{aligned}\Delta G_C^{\gamma\to\alpha} =& K_1(x^i,T) + W_\mu(x^i,T) + W_{HP}(d^\gamma,x^i,T) \\ &+ W_C(d^\gamma,d_c^\gamma,x^i,T) + W_\sigma(x^i,T) + W_\rho(\rho^\gamma,x^i,T)\end{aligned} \tag{4}$$

These contributions are calculated for the austenite state and are respectively linked to the elastic strain and interface energies (K_1), the frictional work due to the solid solution (W_μ), the Hall-Petch strengthening effect (W_{HP}), the change of the martensite lath aspect ratio (W_C), the hydrostatic stress state (W_σ), and the strengthening evolution due to dislocation density (W_ρ). All of these contributions are presented and discussed hereafter in a thermodynamic framework. x^i is the atomic fraction of element i in austenite, T is the temperature, d^γ is the austenite size, d_c^γ is the austenite size threshold value for the aspect lath change ratio, and ρ^γ is the mean dislocation density in austenite.

The proposed model finds its origin in the works of Ghosh and Olson [26, 27]. Their approach is based on the heterogeneous semi-coherent nucleation and growth process of martensite through an energy balance between the thermodynamic driving force and an energy barrier related to the dislocations and interface energy. They used the interphase boundaries description proposed by Olson and Cohen

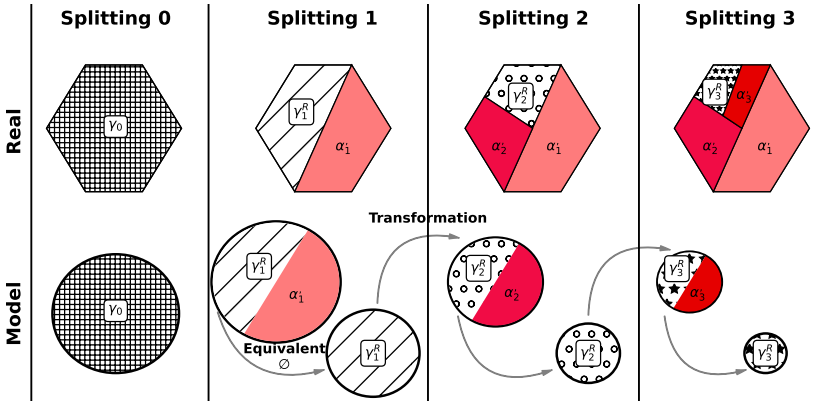

Figure 4: Schematic representation of a grain that undergoes several steps of the martensite transformation as well as the geometrical conversion into an equivalent diameter, keeping the same area at each step.

[65] to estimate the interfacial properties as a semi-coherent FCC/BCC martensitic interface in terms of coherency and anti-coherency dislocations respectively accomplishing the transformation strain and reducing the strain energy.

In recent works [34, 58] K_1 and W_μ were assumed constant to determine the sole Ms temperature, while they are both considered temperature-dependent in this work. Constant K_1 including strain and interfacial energies and defect size is formulated following the Olson and Cohen's interphase boundaries model:

$$K_1 = \left(E^{str} + \frac{2\psi}{nd} \right) V_m^\gamma \tag{5}$$

where E^{str} is the shape-insensitive component of the strain energy associated with the distortions in the nucleus habit plane, ψ is the interfacial energy between the semi-coherent FCC/BCC interface ($\psi = 0.15$ J/m^2), n is the number of close-packed planes comprising the nucleus thickness ($n = 18$), and d is the spacing between close-packed planes ($d = 2.05\times10^{-10}$ m).

Most of the time K_1 is assumed constant and is in order of 1000-1100 J/mol [26,27,34,58]. Nevertheless, as reported by Ghosh and Olson themselves, K_1 is expected to vary with the temperature due to the effect of temperature on the shear modulus [26]. They proposed to take into account the temperature effect on the elastic energy and interface energy as follows [66]:

$$E^{str} = k_{str} S(x^i, T) \tag{6}$$

$$\psi = k_\psi S(x^i, T) \tag{7}$$

where $k_{str} = 9.4\times10^{-4}$ (dimensionless) and $k_\psi = 1.8026\times10^{-12}$ m are proportionality constants [66].

For the athermal frictional work (W_μ) of a martensite interface, Ghosh and Olson assumed that the effect of atoms in solid solution in a multi-components alloy is described by a linear superposition Pythagoeran-type laws [26] accounting for the respective individual effects of each element. Later on, [66], the thermal dependency was taken into account and reads:

$$W_\mu = A_\mu S(x^i, T) V_m^\gamma \tag{8}$$

where $A_\mu = \sqrt{\Sigma (k_\mu^i \sqrt{x_i})^2}$ if only C, Cr, Mn, and Si are considered, V_m^γ is the austenite molar volume, and $S(x^i, T)$ is the shear modulus. k_μ^i are calibration coefficients shown in Table 1.

In the previous Ghosh and Olson's models, the austenite grain size is not taken into account as a feature affecting Ms. This effect was introduced by Van Bohemen and Morsdorf in [34] in order to predict the Ms temperature as a function of the chemical composition and mean PAGS.

The Hall-Petch strengthening (W_{HP}) induced by grain refinement leads to stabilizing mechanically the austenite. The expression used in the present study to describe this effect is derived from these works [34,67,68]. They proposed that the grain interior is softer than the regions close to grain boundaries, which generally show a higher local density of geometrically necessary dislocations. The softest fraction in small grains is lower than the fraction encountered in large grains. As a consequence, small austenite grains oppose a higher resistance to the volume change and to the shear induced by the martensite transformation [68]. Inspired by the works of Hall and Petch, the work opposing the transformation can be described as inversely proportional to the square root of the austenite grain size:

$$W_{HP} = \frac{K_{HP}}{\sqrt{d^{\gamma}}} \tag{9}$$

where K_{HP} is a proportionality constant and d^{γ} is the austenite grain size. In the present study, this expression was also used for austenite domains generated by the progressive splitting process aforementioned.

In a similar framework, Van Bohemen and Morsdorf [34] also took into account the increase of the stored energy due to the formation of martensite laths with a high aspect ratio. It has been experimentally observed that the width of the martensite laths (c) remains almost insensible to the austenite size, whereas the length (l) is proportional to it [34]. So, weak c/l values are generally observed in large austenite grains. When the martensite transformation is constrained by its surroundings, the interface becomes curved to minimize the strain as observed in small grains reducing the number of packets per grain; let us mention that the strain can be also minimized by self-accommodation. The curved interface results in higher stored energy in the austenite at the interface due to the increase of dislocations needed to accommodate the curvature. This result is supported by calculations of elastic strain energies based on Eshelby's theory for an oblate spheroid-like shape as discussed previously [56, 57]. This corresponding stored energy was expressed by [34] as follows:

$$W_C = K_C \exp\left(\frac{-6d^{\gamma}}{d_c^{\gamma}}\right) \tag{10}$$

where K_C is a proportionality constant and d_c^{γ} is a critical austenite grain size. As expected this contribution increases when the grain size or the size of austenitic domain in which the transformation must take place decreases.

Both calibration constants K_{HP} and K_C presented above were fitted using the Ms temperatures of more than 100 alloys with various chemical compositions and grain sizes in [34]. The authors reported $K_{HP} = 0.35$ Jm$^{0.5}$/mol and $K_C = 370$ J/mol. The data used were however limited with a mean Ms temperature of 320 °C (with a minimum at 185 °C and a maximum at 400 °C). As the present study aims to describe the martensite transformation kinetics down to room temperature, the proportionality constants were made dependent on the shear modulus, as done for the K_1 terms [66]. In the present framework, K_{HP} and K_C were expressed as follows:

$$K_{HP} = k_{HP} S(x^i, T) V_m^{\gamma} \tag{11}$$

$$K_C = k_C S(x^i, T) V_m^{\gamma} \tag{12}$$

Both k_{HP} and k_C were evaluated from the mean proportionality constants, the mean Ms temperature (320 °C), and the mean shear modulus at the Ms temperatures (70 GPa) of the investigated alloys in [34]. Thus, $k_{HP} = 7.248\times10^{-4}$ m$^{0.5}$ and $k_C = 7.663\times10^{-4}$ (dimensionless).

It was observed experimentally that, during martensite transformation, internal stresses develop into austenite. These stresses can be a mechanical driving force for further transformation and affect the kinetics as proposed by Patel and Cohen [33] for a martensitic transformation occurring under stress. During martensite transformation, tensile stresses will promote the transformation leading to an increase of Ms whereas hydrostatic compression stresses stabilize the austenite and lead to a decrease of Ms [33,69].

This effect is captured here by the framework proposed originally by [33] considering that during the martensite transformation, austenite is under a mean hydrostatic pressure:

$$W_\sigma(\varepsilon_l^\gamma) = -P\varepsilon_0(T)V_m^\gamma \tag{13}$$

where $P = 3\varepsilon_l^\gamma K(x^i,T)V_m^\gamma$, ε_l^γ is the austenite linear strain as a function of the martensite phase fraction, K is the bulk modulus, $\varepsilon_0(T)$ is the volume change associated with the transformation at a given temperature T, and V_m^γ is the molar volume of austenite. ε_l^γ was determined from the difference of the elastic strain-free and measured austenite lattice parameters during the martensite transformation.

The dislocations induced into the retained austenite during the transformation may assist or counter the martensite transformation. A relatively low increase could help the nucleation of martensite while on the contrary, if the dislocation density is too high, they represent an obstacle for the martensite glissile interface [38]. As there are no well-established criteria to describe the transition, only the stabilizing effect of dislocations is considered following [38]:

$$W_\rho(\rho) = \frac{bS(x^i,T)}{8\pi(1-\nu)}(\sqrt{\rho}-\sqrt{\rho_0})V_m^\gamma \tag{14}$$

where b is the burger vector, ν is the Poisson's ratio, ρ_0 is the dislocation density before the martensite transformation, and ρ is the mean dislocation density in austenite during the martensite transformation.

Even if the evolution of the dislocation density in the austenite can be measured by *in situ* HEXRD experiments, the measured density encompasses the geometrically necessary dislocations (GNDs) and the statistically stored dislocations (SSDs). However, the ratio between GNDs and SSDs cannot be estimated from HEXRD *in situ* experiments. Using the kernel average misorientation, one can decipher the density of GNDs and thus, combined with XRD estimate the ratio. For low-carbon martensitic steels, it appeared that a high fraction of dislocations are GNDs [70,71]. However, the fractions reported correspond to the martensite and there is no report of GNDs in retained austenite only. The GNDs are already considered in the treatment of the stabilization via the formalism used (K_1) [26,27,34], and only the SSDs should be considered as an additional stabilizing factor. Directly applying the dislocation density measured from HEXRD experiments (i.e., including both GNDs and SSDs) would overestimate the stabilizing effect, therefore only a fraction of them would be considered. As the authors did not find any reference about the fraction of GNDs and SSDs in the austenite, it was the authors' choice to incorporate the stabilization caused by the glissile dislocation by considering that 50% of the experimentally determined dislocation density corresponds to SSDs. The selected value is close to the one determined in the martensite [70,71].

4.1.4 Estimation of the chemical driving force

The chemical driving force $\Delta G_{chem}^{\gamma\to\alpha}(T)$ as a function of the temperature for the investigated alloy has been obtained with Thermocalc software and TCFE9 database. The contribution has been approximated by a linear function in the considered temperature range (below Ms). The best linear fit was obtained with the slope of 7.83 J/(mol.K) and T_1 = 588 °C which is coherent with [34]. The results have been plotted in Figure 5. T_1 is the temperature at which the chemical driving force is zero in the linear description. The chemical driving force needed to initiate the martensite transformation of the studied alloy can be evaluated at Ms (365 °C) and is ∼1.7 kJ/mol.

It is remembered that in the present model, the composition is assumed to be homogeneous. However, local variations and segregation, as usually observed, affect the chemical driving force, the solid solution strengthening, and the elastic constants changing locally the Ms temperature and, therefore, the transformation rates. A more complex model would be required to account for the heterogeneities at the grain and dislocation scales.

4.1.5 Parameters of the model

All the parameters used in the present model are taken or derived from the literature and are shown in Table 1. Table 1 presents the coefficients (k_μ^i) used to calculate the frictional work for a martensitic interface based on solid solution strengthening as a function of the temperature taken from [34]. From the investigated steel composition at 365 °C (Ms), W_μ = 575 J/mol and K_1 = 909 J/mol calculated with Equations 5-8 and constants in Table 1 for the present investigated steel. This leads to a critical

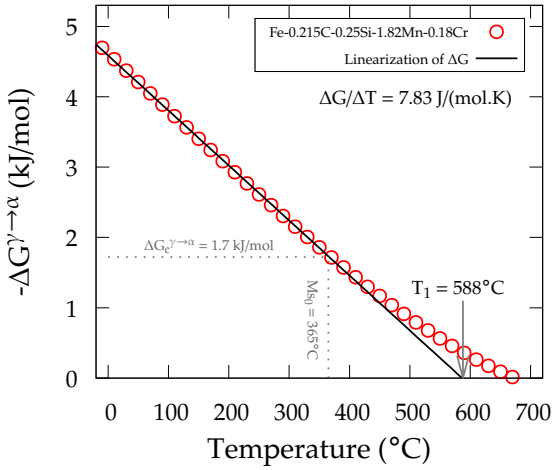

Figure 5: Chemical driving force $\Delta G^{\gamma\rightarrow\alpha}_{chem}(T)$ as a function of the temperature from Thermocalc software and TCFE9 database and the linear extrapolation below Ms used for the calculations.

force of 1484 J/mol which is below the experimental critical force observed (∼1700 J/mol). Accounting for the Hall-Petch (W_{HP}) and stored energy (W_C) effects for a grain size of 14.3 µm, the critical force increases up to 1577 J/mol. This grain size was chosen as it represents the first percent of martensite transformed from our PAGS distribution (i.e. the probability density function (PDF) = 0.99 for d^{γ}(µm) ∈ [0;14.3] and PDF = 0.01 for d^{γ}(µm) ∈ [14.3;+∞]). In order to match the actual Ms temperature and the critical force a constant of 130 J/mol was added to the K_1 constant corresponding to the elastic strain energy and interfacial energy. This is the only adjusted parameter added to the model. Thus, K_1 = 1039 J/mol which is in the range reported in literature [26, 34, 58]. The other input parameters were discussed before. The austenite molar volume was taken equal to those in [51] and considered constant. The volume change associated with the transformation as a function of the temperature was fitted from the data presented in [72] for pure iron. The effect of carbon on lattice parameters of both martensite and austenite and thus on the volume change [73] is not accounted for here, as the magnitude of the volume change is primarily determined by the temperature at which the transformation occurs. At Ms = 365 °C, $\varepsilon_0 = 0.0241$ (Table 1) which is in agreement with the volume change expected for a Fe-0.2C wt% steel at Ms [73]. The isotropic shear modulus of austenite as a function of the composition and temperature was evaluated with the model proposed in [74].

Table 1: Parameters used to model the martensite transformation.

Parameters	Values
k_{μ}^{C} (J/mol)	0.01012
k_{μ}^{Mn} (J/mol)	0.00442
k_{μ}^{Cr} (J/mol)	0.00425
k_{μ}^{Si} (J/mol)	0.00375
k_{str} (dimensionless)	9.4 10^{-4}
k_{ψ} (m)	1.8026 10^{-12}
k_{HP} ($m^{0.5}$)	7.248 10^{-4}
k_C (dimensionless)	7.663 10^{-4}
d_C^{γ} (m)	11 10^{-6}
V_m^{γ} (m^3/mol)	6.9 10^{-6}
ε_0 (dimensionless)	$0.03491 - 3.45 \times 10^{-5}T + 1.37 \times 10^{-8}T^2$
K (J/m^3)	$(2S(1+\nu))/(3(1-2\nu))$
S (J/m^3)	Eq. 16 in [74]
ν (dimensionless)	0.30

4.2 Progress of the martensite transformation

Figure 6 shows the results obtained with the present model, considering the input parameters (Table 1), the PAGS distribution (Figure 1), the mean austenite strain, and dislocation density (Figure 2); (a) each individual contribution to the critical resistive forces stabilizing progressively the austenite as a function of the simulated martensite phase fraction and (b) the predicted martensite transformation as a function of the temperature difference compared to Ms accounting for the different work contributions and the experimental martensite phase fraction. In Figure 6a, each contribution increases with the progress of the martensite transformation and temperature decrease, stabilizing the untransformed austenite. The resulting increase of the strain and interface energies (K_1) and athermal frictional work (W_μ) are solely due to the increase of the shear modulus with the temperature decrease. The Hall-Petch strengthening effect is the major contribution and reaches high values at the end of the transformation due to the very low grain size. Figure 6b shows that the evolution of AGS distribution allows explaining the kinetics observed up to ~50-60 % of formed martensite. The dislocation contribution is directly related to the increase of the dislocation density and its effect on the kinetics is mainly observed during the second half of the transformation. The stress effect appears to be weak until 70 % of martensite is transformed. In the absence of the stabilization of austenite, the transformation evolution should be a vertical straight line at Ms. These results show that the major contribution to the spread of the martensite transformation is the size reduction and distribution of the austenite domains (W_{HP} and W_C terms).

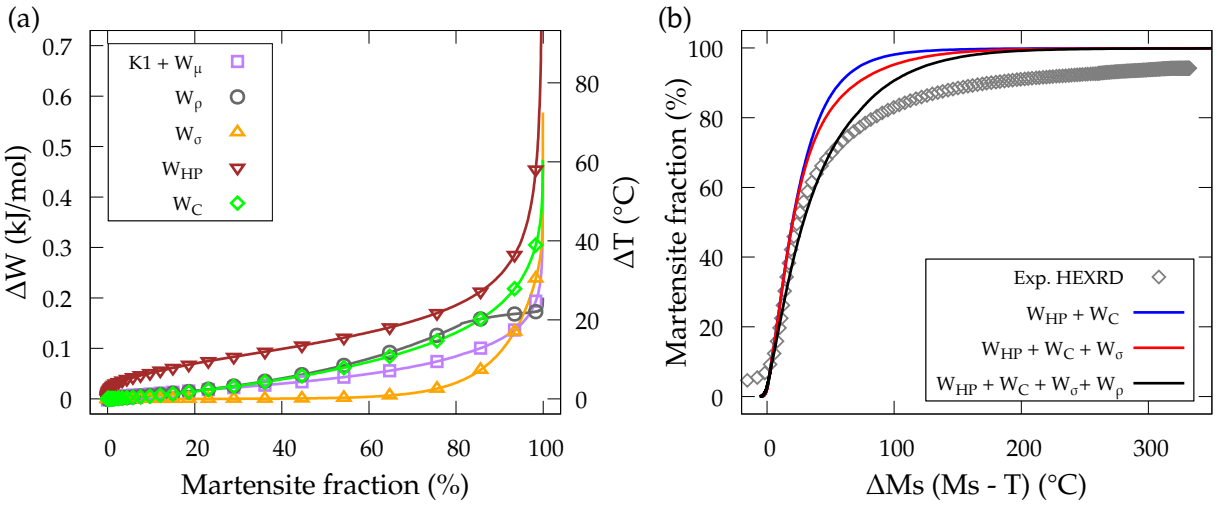

Figure 6: (a) Individual variations of the contributions stabilizing the austenite as a function of the simulated martensite phase fraction and (b) experimental and simulated martensite phase fractions as a function of the temperature difference as compared to Ms.

5 Discussion

5.1 Limitations of the current approach

The approach used in the present study captures well the nature of the martensite transformation solely based on a thermodynamic stabilization of austenite. However, discrepancies persist between the calculation and the experiment. At room temperature, a small fraction of retained austenite is predicted by the model (~1 %); this fraction is lower than the experimentally measured one (~4 %). In addition, the kinetics rate parameter is over-estimated above 60 % of martensite transformed. The current model considers that stresses are homogeneously distributed, which is far certainly from reality [23, 75]. The martensite transformation process is much more complex than the geometric model presented here, e.g., the crystal orientation relationships and martensite variants are not presently considered in the refinement model as well as the grain geometry. The formation of GNDs accommodating the transformation is accounted for in the present model through K_1 [26, 27]. The effect of the SSDs, representing an obstacle for the martensite glissile transformation interface [38], has been also accounted for by Equation 14. However,

the dislocation density evolution was determined by an *in situ* HEXRD experiment compassing GNDs and SSDs. To the authors' knowledge, no precise information regarding the fraction of each dislocation kind is available in the literature for the austenite. Therefore, an assumption that 50 % of dislocation density (i.e., GNDs + SSDs) measured in austenite during the transformation [24] represents an obstacle using Equation 14 has been made. Up to 90 % of the transformation, it can be observed that the contribution due to dislocations is close to that due to the aspect ratio. At this point, the stabilization due to dislocations reaches a kind of plateau related to the measured dislocation density. All the others show an asymptotic increase. Therefore, when accounting for the stabilization due to the dislocations, the transformation kinetics are retarded up to 200 °C below Ms, see Figure 6b. It can also be observed that, even if the contribution of the dislocations is overestimated, no effect on the final martensite fraction is predicted. Additional calculations with different fractions of SSDs, from 0 % up to 100 %, are presented in Supplementary Material B showing the effect of SSDs on the kinetic of martensite transformation. However, varying the fraction of SSDs from 25 % to 100 % presents a small effect.

In order to test the refinement model, the retained austenite mean equivalent diameter is compared with measured ones from the literature [59]. The refinement model presented here was applied to the PAGS distributions reported by the authors up to 68 % of martensite formed (after austenitization at 900 °C) leading to obtaining the retained austenite mean size at this given phase fraction. The values calculated are between ten to more than twenty times higher (e.g., the authors reported a mean retained austenite size of 0.73 µm while the refinement model calculated 7.8 µm). This size difference leads to a discrepancy in the strengthening effect and stored energy contributions calculations. The difference corresponds to 548 J/mol which represents an absolute Ms variation of ∼70 °C assuming a linear driving force as a function of the temperature of 7.83 J/(mol.K) and the shear modulus at room temperature. The austenite domain sizes are overestimated by the refinement model used, therefore, affecting the evaluation of the austenite stability. Both deeper experimental analysis of austenite domain sizes and a more complex model would be required to go further.

5.2 Effect of alloying element on the kinetics of martensite transformation

It is reported in the literature that allowing elements affect the rate parameter (α in Koistinen-Marburger's law, Equation 1) of the martensite transformation [40, 76, 77]. As investigated in [40, 41, 77] the increase of carbon and alloying elements decreases the rate parameter, which means that a higher under-cooling is needed to obtain a given martensite phase fraction. The change of the rate parameter with the composition was said six decades ago to be proportional to the change of the driving force with the temperature [76]. Here, first, the effect of alloying elements on the chemical driving force will be quantified, and then their effect on the rate parameter. Thermodynamic calculations were first performed using Thermocalc software and TCFE9 database considering binary systems (Fe-X where X is C up to 0.8 wt %, Mn, Si, Cr, Ni, and Mo up to 6 wt %). Afterward, the chemical driving force as a function of the temperature for each composition was fitted with a linear relationship (as formerly presented in Figure 5) in the temperature range 0 to 400 °C in order to obtain the influence of alloying element on the slope of the driving force and thus on the martensite transformation rate. The T_1 temperature evolution as a function of the alloying element was investigated as well. Results are shown in Table 2.

The first outcome is that the elements investigated decrease the slope of the driving force as a function of the temperature, leading to the spread of the martensite transformation. The major effect is found for the C element. These results confirm the literature [40, 41, 77]. It has to be mentioned that the driving force as a function of the temperature presents a linear relationship with all the elements in the investigated range (supporting previous analysis [41, 77]). Similar observations are made for the T_1 temperature, except that both Si and Mo contribute to the increase in the temperature. Mention that both the influence of the alloying elements on the slope and the T_1 temperature can be used to refine the Ms temperature prediction via the thermodynamic-based model presented in [34].

In a second time, the evolution of the rate parameter was investigated with the model by making vary the driving force as a function of the temperature with the composition. In these calculations, the PAGS distribution, the mean hydrostatic stress, and the dislocation density effects used before were considered and kept similar. Thus, the differences observed are related to a change in chemical composition. Figure 7 shows the kinetics calculated for different C, Mn, and Cr contents. Only these three elements are presented as they showed the largest effect on the driving force (Table 2). As previously mentioned, carbon shows the main effect on the kinetics of martensite transformation compared to the other elements. The results

Table 2: Influence of the alloying elements on the slope and the T_1 temperature of the austenite to ferrite driving force as a function of the temperature for binary alloys. The slope of the driving force as a function of the temperature for iron is 8.4268 J/(mol.K) in the temperature range from 0 to 400 °C. The T_1 temperature for iron is 937 K.

Element	C	Mn	Cr	Ni	Si	Mo
J/(mol.K.wt %)	-1.620	-0.109	-0.102	-0.070	-0.035	-0.016
K/(wt %)	-230	-18	-3.6	-12.5	+0.7	+2.4

show that the rate of the martensite transformation is related to the composition of the steel. Indeed, the higher the alloying content, the lower the slope of the driving force as a function of the temperature and thus the lower the transformation kinetics. However, for elements such as Si, the influence on the slope of the austenite to ferrite driving force as a function of the temperature is negligible, but its effect on shear modulus can be important [74]. As a consequence, the kinetic rate will be faster because of the lower resistive forces due to a lower shear modulus, which is considered in each resistive force of this work.

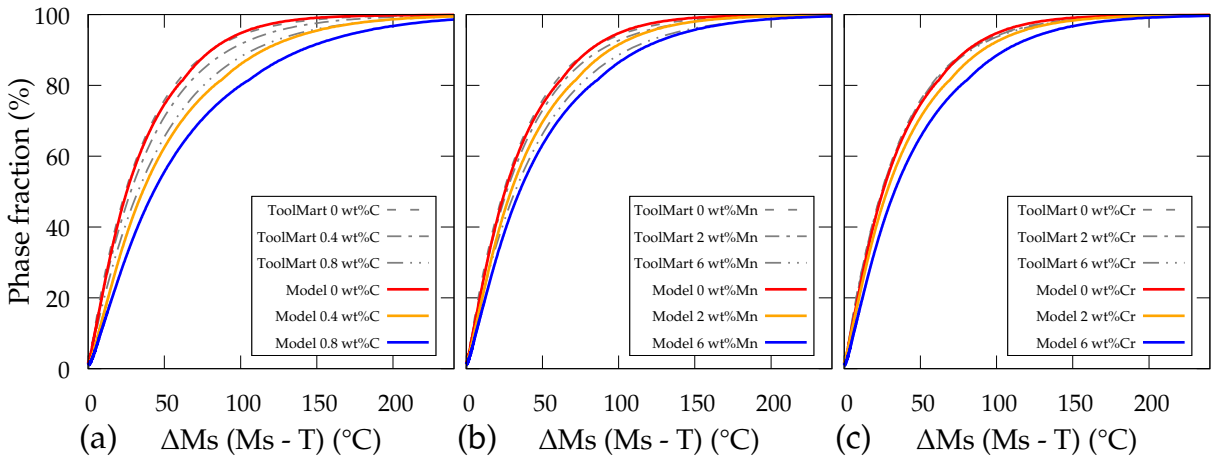

Figure 7: Influence of the composition on the computed martensite transformation kinetics: (a) carbon, (b) manganese, and (c) chromium content of a binary Fe-X alloy. The results are compared with the empirical model presented in ToolMart [41].

The results of the present model are compared with kinetics calculated with the phenomenological model presented in [41] (Figure 7). The exponent term $m = 0.892$ allowing to take into account the mean PAGS on the rate parameter [41] was adjusted to fit the calculated martensite transformation (see Supplementary Material C). It is observed that only Mn effect is close to the one predicted by the phenomenological model. For both C and Cr alloying elements, the kinetics slowdown calculated with our model is higher than the ones reported with the phenomenological model. This is explained by the restricted range of carbon (0.14 to 0.22 wt %) and chromium (0.2 to 2 wt %) composition of steels used to develop the phenomenological model. The kinetics predicted by the model were fitted with the phenomenological model in order to obtain new $\Delta\alpha$ coefficients depending on the alloying elements ($\alpha = \alpha_0 + \sum_i w^i \Delta\alpha^i$). The $\Delta\alpha$ coefficients for C, Mn, and Cr proposed are respectively $\Delta\alpha^C$ = -0.058/(K.wt %), $\Delta\alpha^{Mn}$ = -0.0035/(K.wt %), and $\Delta\alpha^{Cr}$ = -0.0035/(K.wt %). For C, the coefficient reported is higher to an anterior work in which PAGS was not considered [77] but smaller than in [41].

The current work shows that variations observed in the rate parameter (α) of the Koistinen-Marburger equation to describe the martensite transformation as a function of the under-cooling below the martensite temperature can be explained by a thermodynamic approach and is the consequence of the change of the chemical driving force related to the steel composition.

6 Conclusion

In the present work, a model to describe the kinetic of the martensite transformation based on the stabilization of the austenite during the transformation is presented. The stabilization of austenite is described in a thermodynamic framework taking into account the chemical composition, grain size, stress state, dislocation density, and temperature effects which were not all considered together before to describe the transformation. The proposed theoretical development relies on some experimental results gathered on low-alloyed steels and on a simple grain partition model which is introduced to predict the evolution of the AGS during the transformation. In addition to the model development, *in situ* high-energy X-ray diffraction experiments were performed at the DESY synchrotron allowing us to obtain the microstructural evolution occurring during the transformation such as the phase fractions, the mean austenite lattice parameter as well as the evolution of the austenitic mean dislocation density. These results have been used to test the validity of our theoretical description of the martensite transformation.

The model predicted the transformation kinetic with a good agreement up to 60-70 % of the martensite transformation upon cooling and showed that the major contribution to the spread of the transformation is the austenite refinement during the transformation itself. The discrepancies between the model and the experiment above 60-70 % have been attributed mainly to austenite refinement, which is not accurately captured by the simple description used. A better knowledge of the local internal stresses would also be necessary.

Then, the model was used to investigate the relative effect of alloying elements on the progress of the transformation rate. The results showed that the rate of the progress of a martensite transformation is linked with the change of the chemical driving force related to the steel composition. Among the alloying elements investigated, C showed the highest effect as observed for the Ms temperature. Based on the numerical results, new coefficients for the rate parameter (α) of the martensite transformation were proposed to be used with a phenomenological approach of the martensite transformation.

The current work has presented a new perspective to better understand the martensite transformation and the progress of the transformation rate associated with the stabilization of austenite instead of describing the nucleation processes of each individual unit of martensite. Although based on a low-alloyed steel, the developed framework presents a good extensibility, as the parameters used were not adjusted, to describe the kinetics and can be applied on a large panel of martensitic steels.

Author contributions: Conceptualization, S.G, J.M., S.D., S.Y.P.A; investigation, S.G., J.M., G.G.; writing-original draft preparation, S.G., J.M.; writing-review and editing, S.G, J.M. G.G., S.D., S.Y.P.A; supervision, S.D., S.Y.P.A; project administration, S.Y.P.A; funding acquisition, S.Y.P.A. All authors have read and agreed to the published version of the manuscript.

Acknowledgments: This work was funded by the i-SITE Lorraine Université d' Excellence program (LUE) and supported by ArcelorMittal Maizières-les-Metz (Product Research Centre). The HEXRD experiments were conducted at DESY (PETRAIII-P07 beamline) in Hamburg under the I-20180973 EC grant. A special thanks is dedicated to the team of the P-07 line. The expertise of N. Schell and A. Stark was much appreciated and widely contributed to the success of the study. The Laboratory of Excellence on Design of Alloy Metals for low-mAss Structures (Labex DAMAS) from the Université de Lorraine (France) is acknowledged for its support.

Conflicts of interest: On behalf of all authors, the corresponding author states that there is no conflict of interest. The funders had no role in the design of the study; in the collection, analyses, or interpretation of data; in the writing of the manuscript, or in the decision to publish the results.

Data availability: The raw/processed data required to reproduce these findings cannot be shared at this time, as the data also forms part of an ongoing study.

References

[1] E. Pereloma and D.V. Edmonds. Phase transformations in steels: Diffusionless transformations, high strength steels, modelling and advanced analytical techniques. Elsevier, 2012.

[2] G. Badinier, C.W. Sinclair, S. Allain, F. Danoix, and M. Gouné. The mechanisms of transformation and mechanical behavior of ferrous martensite. In Reference Module in Materials Science and Materials Engineering. Elsevier, 2017.

[3] S Banerjee and R Krishnan. Martensitic transformation in zirconium-niobium alloys. Acta Metallurgica, 19(12):1317–1326, 1971.

[4] B. Strauss, F. Frey, W. Petry, J. Trampenau, K. Nicolaus, S. M. Shapiro, and J. Bossy. Martensitic phase transformation and lattice dynamics of fcc cobalt. Physical Review B, 54:6035–6038, Sep 1996.

[5] T. Ahmed and H.J. Rack. Phase transformations during cooling in α+β titanium alloys. Materials Science and Engineering: A, 243(1):206–211, 1998.

[6] J. Lang and A.R. Williams. The hardening of iron swords. Journal of archaelogical science, 2(3):199–207, 1975.

[7] J. Lang. Study of the metallography of some roman swords. Britannia, 19:199–216, 1988.

[8] A. Shibli and F. Starr. Some aspects of plant and research experience in the use of new high strength martensitic steel P91. International Journal of Pressure Vessels and Piping, 84(1):114–122, 2007. Development of and Integrity Issues with New High Temperature High Strength Steels.

[9] C.D.J. Barras and K.A. Myers. Nitinol – its use in vascular surgery and other applications. European Journal of Vascular and Endovascular Surgery, 19(6):564–569, 2000.

[10] S. Aoued, F. Danoix, S.Y.P. Allain, S. Gaudez, G. Geandier, J.C. Hell, M. Soler, and M. Gouné. Microstructure evolution and competitive reactions during quenching and partitioning of a model Fe–C–Mn–Si alloy. Metals, 10(1), 2020.

[11] J. Speer, D.K. Matlock, B.C. De Cooman, and J.G. Schroth. Carbon partitioning into austenite after martensite transformation. Acta Materialia, 51(9):2611–2622, 2003.

[12] N. Fonstein. 7 - dual-phase steels. In Radhakanta Rana and Shiv Brat Singh, editors, Automotive Steels, pages 169–216. Woodhead Publishing, 2017.

[13] G. Krauss. Martensite in steel: strength and structure. Materials Science and Engineering: A, 273-275:40–57, 1999.

[14] P.K. Tripathi, S. Karewar, Y.C. Lo, and S. Bhowmick. Role of interface morphology on the martensitic transformation in pure Fe. Materialia, 16:101085, 2021.

[15] S. Karewar, J. Hidalgo, J. Sietsma, and M.J. Santofimia. Role of planar faults in martensite formation in nano-polycrystalline iron by molecular dynamics simulation. Journal of Materials Science, 57(37):17678–17699, 2022.

[16] Z.Z. Wei, X. Ma, C.B. Ke, and X.P. Zhang. Distinct migration mechanisms of stepped FCC/BCC martensitic interfaces associated with typical orientation relationships: a molecular dynamics study. Journal of Materials Science, 57(42):19857–19871, 2022.

[17] C. Cayron. Continuous atomic displacements and lattice distortion during fcc–bcc martensitic transformation. Acta Materialia, 96:189–202, 2015.

[18] C. Cayron. Shifting the shear paradigm in the crystallographic models of displacive transformations in metals and alloys. Crystals, 8(4), 2018.

[19] P.M. Kelly. 1 - crystallography of martensite transformations in steels. In E. Pereloma and D.V. Edmonds, editors, Phase Transformations in Steels, volume 2 of Woodhead Publishing Series in Metals and Surface Engineering, pages 3–33. Woodhead Publishing, 2012.

[20] P Maugis. A temperature–stress phase diagram of carbon-supersaturated bcc-iron, exhibiting "beyond-zener" ordering. Journal of Phase Equilibria and Diffusion, 41:269–275, 2020.

[21] A. Shibata, T.Murakami, S. Morito, T. Furuhara, and T. Maki. The origin of midrib in lenticular martensite. Materials Transactions, 49(6):1242–1248, 2008.

[22] S. Morito, Y. Edamatsu, K. Ichinotani, T. Ohba, T. Hayashi, Y. Adachi, T. Furuhara, G. Miyamoto, and N. Takayama. Quantitative analysis of three-dimensional morphology of martensite packets and blocks in iron-carbon-manganese steels. Journal of Alloys and Compounds, 577:S587–S592, 2013. SI :ICOMAT2011.

[23] N. Nakada, Y. Ishibashi, T. Tsuchiyama, and S. Takaki. Self-stabilization of untransformed austenite by hydrostatic pressure via martensitic transformation. Acta Materialia, 110:95–102, 2016.

[24] J. Macchi, S. Gaudez, G. Geandier, J. Teixeira, S. Denis, F. Bonnet, and S.Y.P. Allain. Dislocation densities in a low-carbon steel during martensite transformation determined by in situ high energy x-ray diffraction. Materials Science and Engineering: A, 800:140249, 2021.

[25] S. Gaudez, J. Teixeira, S. Denis, G. Geandier, and S.Y.P. Allain. Martensite and nanobainite transformations in a low alloyed steel studied by in situ high energy synchrotron diffraction. Materials Characterization, 185:111740, 2022.

[26] G. Ghosh and G.B. Olson. Kinetics of f.c.c. → b.c.c. heterogeneous martensitic nucleation—i. the critical driving force for athermal nucleation. Acta Metallurgica et Materialia, 42(10):3361–3370, 1994.

[27] G. Ghosh and G.B. Olson. Kinetics of f.c.c. → b.c.c. heterogeneous martensitic nucleation—ii. thermal activation. Acta Metallurgica et Materialia, 42(10):3371–3379, 1994.

[28] E.I. Galindo-Nava. On the prediction of martensite formation in metals. Scripta Materialia, 138:6–11, 2017.

[29] ES Machlin and M. Cohen. Burst phenomenon in the martensitic transformation. JOM, 3(9):746–754, 1951.

[30] A.R. Entwisle. The kinetics of martensite formation in steel. Metallurgical transactions, 2(9):2395–2407, 1971.

[31] Y. Li, D. San Martín, J. Wang, C. Wang, and W. Xu. A review of the thermal stability of metastable austenite in steels: Martensite formation. Journal of Materials Science & Technology, 91:200–214, 2021.

[32] W. Gong, S. Harjo, Y. Tomota, S. Morooka, T. Kawasaki, A. Shibata, and N. Tsuji. Lattice parameters of austenite and martensite during transformation for Fe–18Ni alloy investigated through in-situ neutron diffraction. Acta Materialia, page 118860, 2023.

[33] J.R. Patel and M. Cohen. Criterion for the action of applied stress in the martensitic transformation. Acta Metallurgica, 1(5):531–538, 1953.

[34] S.M.C. van Bohemen and L. Morsdorf. Predicting the Ms temperature of steels with a thermodynamic based model including the effect of the prior austenite grain size. Acta Materialia, 125:401–415, 2017.

[35] S. Ebner, C. Suppan, A. Stark, R. Schnitzer, and C. Hofer. Austenite decomposition and carbon partitioning during quenching and partitioning heat treatments studied via in-situ x-ray diffraction. Materials & Design, 178:107862, 2019.

[36] M.J. Santofimia, J.G. Speer, A.J. Clarke, L. Zhao, and J. Sietsma. Influence of interface mobility on the evolution of austenite–martensite grain assemblies during annealing. Acta Materialia, 57(15):4548–4557, 2009.

[37] N. Maruyama, S. Tabata, and H. Kawata. Excess solute carbon and tetragonality in as-quenched Fe-1Mn-C (C: 0.07 to 0.8 mass pct) martensite. Metallurgical and Materials Transactions A, 51(3):1085–1097, 2020.

[38] S. Chatterjee, H.S. Wang, J. R. Yang, and H.K.D.H. Bhadeshia. Mechanical stabilisation of austenite. Materials Science and Technology, 22(6):641–644, 2006.

[39] D.P. Koistinen and R.E. Marburger. A general equation prescribing the extent of the austenite-martensite transformation in pure iron-carbon alloys and plain carbon steels. Acta Metallurgica, 7(1):59–60, 1959.

[40] S.M.C. van Bohemen. Bainite and martensite start temperature calculated with exponential carbon dependence. Materials Science and Technology, 28(4):487–495, 2012.

[41] S.M.C. Van Bohemen, L Morsdorf, Collet, M. Caruso, I. Tolleneer, C. Georgesand S. Cobo B, and L. Bracke C. New metallurgical tools for optimum design of modern ultra high strength low carbon martensitic steels (TOOLMART). Technical report, Research fund for coal and steel, 2018.

[42] M. Cohen. Martensitic nucleation-revisited. Materials Transactions, JIM, 33(3):178–183, 1992.

[43] Y. Li, L. Wang, K. Zhu, C. Wang, and W. Xu. An integral transformation model for the combined calculation of key martensitic transformation temperatures and martensite fraction. Materials & Design, 219:110768, 2022.

[44] S.Y.P. Allain, O. Bouaziz, and M. Takahashi. Toward a new interpretation of the mechanical behaviour of as-quenched low alloyed martensitic steels. ISIJ International, 52(4):717–722, 2012.

[45] M.C. McGrath, D.C. Van Aken, N.I. Medvedeva, and J.E. Medvedeva. Work hardening behavior in steel with multiple TRIP mechanisms. Metallurgical and Materials Transactions A, 44(10):4634–4643, 2013.

[46] L. Morsdorf, O. Jeannin, D. Barbier, M. Mitsuhara, D. Raabe, and C.C. Tasan. Multiple mechanisms of lath martensite plasticity. Acta Materialia, 121:202–214, 2016.

[47] L.Y. Wang, Y.X. Wu, W.W. Sun, Y. Bréchet, L. Brassart, A. Arlazarov, and C.R. Hutchinson. Strain hardening behaviour of as-quenched and tempered martensite. Acta Materialia, 199:613–632, 2020.

[48] J. Kieffer and D. Karkoulis. PyFAI, a versatile library for azimuthal regrouping. Journal of Physics: Conference Series, 425(20):202012, mar 2013.

[49] C. García de Andrés, F.G. Caballero, C. Capdevila, and D. San Martín. Revealing austenite grain boundaries by thermal etching: advantages and disadvantages. Materials Characterization, 49(2):121–127, 2002.

[50] S.M.C. van Bohemen. The nonlinear lattice expansion of iron alloys in the range 100–1600K. Scripta Materialia, 69(4):315–318, 2013.

[51] S.Y.P. Allain, S. Gaudez, G. Geandier, J.C. Hell, M. Gouné, F. Danoix, M. Soler, S. Aoued, and A. Poulon-Quintin. Internal stresses and carbon enrichment in austenite of quenching and partitioning steels from high energy x-ray diffraction experiments. Materials Science and Engineering: A, 710:245–250, 2018.

[52] C. Kittel. Introduction to solid state physics. John Wiley & sons, inc, 2005.

[53] F. Bruneseaux. Apport de la diffraction des rayons X à haute énergie sur les transformations de phases, application aux alliages de titanes. PhD thesis, Institut National Polytechnique de Lorraine, 2008.

[54] M Dehmas, F Bruneseaux, G Geandier, E Gautier, B Appolaire, S Denis, B Denand, A Settefrati, A Mauro, M Peel, et al. Apport de la diffraction synchrotron à l'étude de la transformation martensitique dans les aciers. Matériaux & Techniques, 97:61–69, 2009.

[55] M. Villa, F. Niessen, and M.A.J. Somers. In situ investigation of the evolution of lattice strain and stresses in austenite and martensite during quenching and tempering of steel. Metallurgical and Materials Transactions A, 49(1):28–40, 2018.

[56] J. Christian. Thermodynamics and kinetics of martensite. In Proceedings of the international conference on martensitic transformations ICOMAT, 1979.

[57] T. Mura. Micromechanics of defects in solids. Springer Science & Business Media, 2013.

[58] C. Celada-Casero, J. Sietsma, and M.J. Santofimia. The role of the austenite grain size in the martensitic transformation in low carbon steels. Materials & Design, 167:107625, 2019.

[59] M. Agnani, O.L. DeNonno, K.O. Findley, and S.W. Thompson. Quantitative analysis of microstructural refinement in simulated carburized microstructures. Journal of Materials Engineering and Performance, 29(6):3551–3559, 2020.

[60] E. Gautier, J. Zhang, Y. Wen, and S. Denis. Effects of stress on martensitic transformation in ferrous alloys. experiments and numerical simulations. In Phase Transformations and Evolution in Materials as held at the 2000 TMS Annual Meeting, pages 291–306, 2000.

[61] J.R.C. Guimarães and P.R. Rios. Unified model for plate and lath martensite with athermal kinetics. Metallurgical and Materials Transactions A, 41(8):1928–1935, 2010.

[62] J.R.C. Guimarães and P.R. Rios. Spatial aspects of martensite. Metallurgical and Materials Transactions A, 43(7):2218–2224, 2012.

[63] S. Morito, H. Saito, T. Ogawa, T. Furuhara, and T. Maki. Effect of austenite grain size on the morphology and crystallography of lath martensite in low carbon steels. ISIJ International, 45(1):91–94, 2005.

[64] T. Furuhara, K. Kikumoto, H. Saito, T. Sekine, T. Ogawa, S. Morito, and T. Maki. Phase transformation from fine-grained austenite. ISIJ International, 48(8):1038–1045, 2008.

[65] G.B. Olson and M. Cohen. A mechanism for the strain-induced nucleation of martensitic transformations. Journal of the Less Common Metals, 28(1):107–118, 1972.

[66] G Ghosh and G.B. Olson. Computational thermodynamics and the kinetics of martensitic transformation. Journal of Phase Equilibria, 22(3):199–207, 2001.

[67] E.M. Breinan and G.S. Ansell. The influence of austenite strength upon the austenite-martensite transformation in alloy steels. Metallurgical Transactions, 1(6):1513–1520, 1970.

[68] P.J. Brofman and G.S. Ansell. On the effect of fine grain size on the Ms temperature in Fe-27Ni-0.025C alloys. Metallurgical transactions A, 14(9):1929–1931, 1983.

[69] S. Denis, E. Gautier, A. Simon, and G. Beck. Stress–phase-transformation interactions – basic principles, modelling, and calculation of internal stresses. Materials Science and Technology, 1(10):805–814, 1985.

[70] M. Shamsujjoha. Evolution of microstructures, dislocation density and arrangement during deformation of low carbon lath martensitic steels. Materials Science and Engineering: A, 776:139039, 2020.

[71] J. Macchi. Phase transformations, microstructure heterogeneities and resulting mechanical properties in as-quenched and tempered martensitic steels. Theses, Université de Lorraine, December 2022.

[72] Z.S. Basinski, W. Hume-Rothery, and A.L. Sutton. The lattice expansion of iron. Proceedings of the Royal Society of London. Series A. Mathematical and Physical Sciences, 229(1179):459–467, 1955.

[73] J.M. Moyer and G.S. Ansell. The volume expansion accompanying the martensite transformation in iron-carbon alloys. Metallurgical Transactions A, 6:1785–1791, 1975.

[74] G. Ghosh and G.B. Olson. The isotropic shear modulus of multicomponent Fe-base solid solutions. Acta Materialia, 50(10):2655–2675, 2002.

[75] J. Kundin, D. Raabe, and H. Emmerich. A phase-field model for incoherent martensitic transformations including plastic accommodation processes in the austenite. Journal of the Mechanics and Physics of Solids, 59(10):2082–2102, 2011.

[76] R. Brook, A.R. Entwisle, and E.F. Ibrahim. The effect of chemical composition on the shape of martensite transformation curves. Journal of the Iron and Steel Institute, pages 292–298, 1960.

[77] S.M.C. van Bohemen and J. Sietsma. Effect of composition on kinetics of athermal martensite formation in plain carbon steels. Materials Science and Technology, 25(8):1009–1012, 2009.

Supplementary of

Thermodynamic approach to describe the martensite phase transformation kinetics via the stabilization of austenite

Steve Gaudez[1,*], Juan Macchi[1,**], Guillaume Geandier[1], Sabine Denis[1], Sébastien Y.P. Allain[1]
[1] Institut Jean Lamour, UMR 7198 CNRS-Université de Lorraine, 54011 Nancy, France

Corresponding author emails: * steve.gaudez@psi.ch, ** juan.macchi@univ-rouen.fr

A. Austenite grain size distribution management

The management of the Austenite Grain Size (AGS) distribution during the transformation is presented in Figure S1. The initial distribution is characterized by N classes with a constant interval and for each a Probability Density (PD), the sum of the PD is one. Let us consider the transformation in the N class at the first step. The fraction of martensite formed (red part in Figure S1) is the product of the probability density of the class N by the fixed fraction of martensite transformed at each step (δf).

$$PD(N)^{\alpha'} = PD(N)\delta f \tag{S1}$$

Thus, the remaining austenite (blue in Figure S1) reads:

$$PD(N)^{\gamma} = PD(N)(1-\delta f) \tag{S2}$$

To redistribute the remaining austenite in the AGS distribution, its size is calculated assuming a circular morphology:

$$A_N^{\gamma} = \frac{\pi (d_N)^2}{4}(1-\delta f) \tag{S3}$$

$$d_N^{\gamma} = \sqrt{\frac{4A_N^{\gamma}}{\pi}} \tag{S4}$$

where A_N^{γ} is the area of the remaining austenite of the grain d_N and d_N^{γ} its equivalent diameter.

Finally, $PD(N)^{\gamma}$ is added to a class j corresponding to the diameter d_N^{γ}.

$$PD(j)^{final} = PD(j)^{initial} + PD(N)^{\gamma} \tag{S5}$$

where $PD(j)^{initial}$ is the probability density before the redistribution and $PD(j)^{final}$ is the probability density after the redistribution.

These calculations and redistribution are repeated at each step of the transformation until the last class (j=0) which stands for the end of martensite transformation (100%).

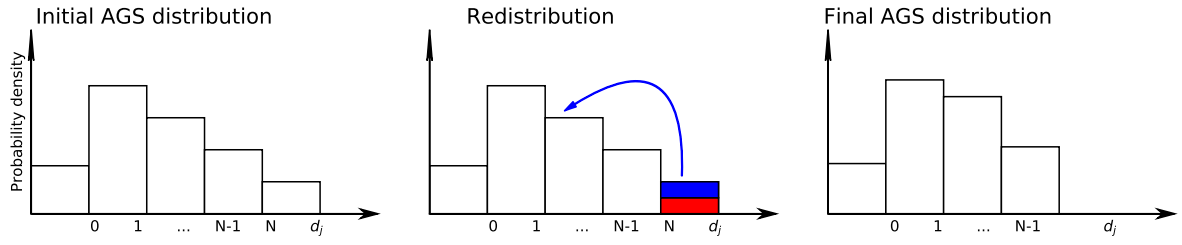

Figure S1: Representation of the austenite grain size redistribution during one step of the transformation (red color represents the fraction of martensite transformed and the blue color represents the remaining austenite of the grain N).

B. Effect of SSDs fraction

Figure S2 shows the effect of the SSDs fraction on the kinetics of the martensite transformation. The density of SSDs in austenite ρ^{γ}_{SSDs} is calculated as:

$$\rho^{\gamma}_{SSDs} = k\rho^{\gamma}_{Tot} \tag{S6}$$

where k is a proportionality factor ranging from 0% to 100% and ρ^{γ}_{Tot} the dislocation density encompassing both SSDs and GNDs measured experimentally and presented in Figure 2b.

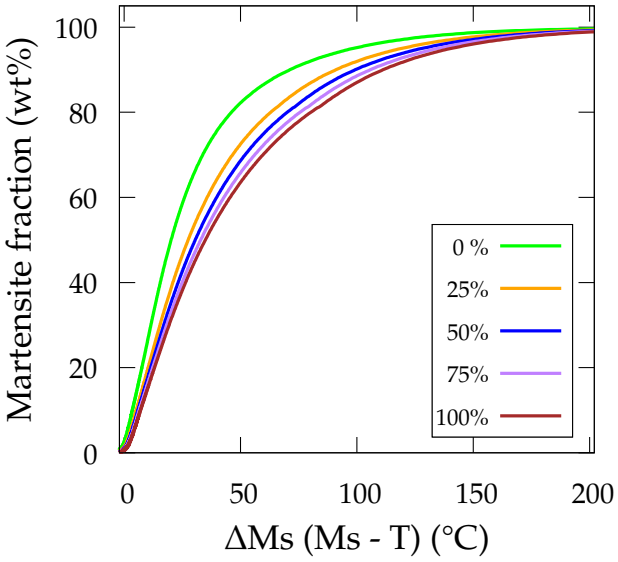

Figure S2: Effect of the SSDs fraction on the kinetic of the martensite transformation.

C. Determination of the KM equation parameter

In order to compare the effect of alloying elements on the kinetics of martensite transformation predicted by our model, the parameter m of the phenomenological model of martensite transformation in ToolMart [41] was adjusted to the martensite transformation predicted by the numerical model considering a pure iron and a mean PAGS of 4.8 µm. The rate parameter (α_{KM}) is defined as:

$$\alpha_{KM} = (0.0255 + \Delta\alpha^i w^i) \times (1 + 6.5\exp(-(d_\gamma)^m)) \tag{S7}$$

where α_{KM} is the rate parameter, $\Delta\alpha^i$ is composition dependency coefficients, w^i is the composition in wt% of the element i, d_γ is the mean PAGS, and m a fitting parameter related to the mean austenite grain size.

For an iron with $d_\gamma = 4.8$ µm the rate parameter reads:

$$\alpha_{KM} = 0.0255 \times (1 + 6.5\exp(-4.8^m)) \tag{S8}$$

Figure S3 shows the best fitting between the computed martensite transformation considering a pure iron and PAGS showed Figure 1 in the paper and the modeled martensite transformation with Equation S8. This was obtained with $m = 0.892$. The effect of alloying elements on the kinetic of martensite transformation predicted by the numerical model has been compared with the phenomenological model [41] in Figure 7 using:

$$\alpha_{KM} = (0.0255 - 0.008C - 0.001Mn - 0.00012Cr) \times (1 + 6.5exp(-4.8^{0.892})) \tag{S9}$$

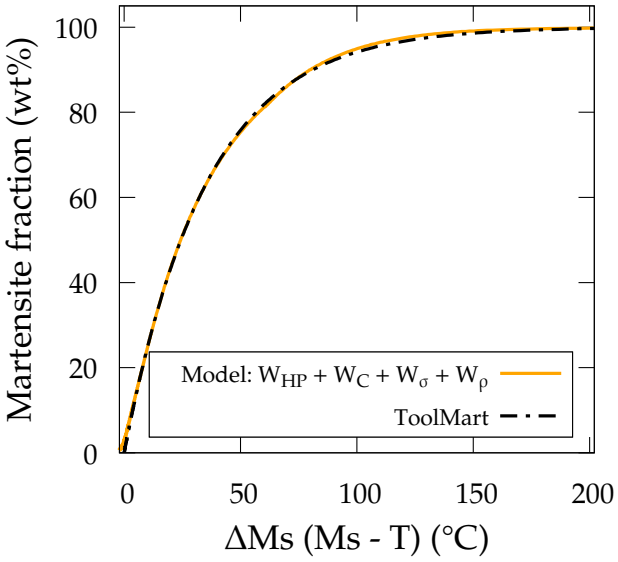

Figure S3: Experimental HEXRD martensite fraction and the fitted progress of transformation following the model proposed in [41] with the parameter m fitted to 0.4928 and Ms = 550 °C.